Molecular Cell, Vol. 23, 113–124, August 4, 2006 ©2006 Elsevier Inc. DOI 10.1016/j.molcel.2006.05.039

Crystal Structure of the PP2A Phosphatase Activator: Implications for Its PP2A-Specific PPIase Activity

Nicolas Leulliot,[1,5] Giorgia Vicentini,[2,5] Jan Jordens,[3,5] Sophie Quevillon-Cheruel,[1] Marc Schiltz,[4] David Barford,[2,6] Herman Van Tilbeurgh,[1,7] and Jozef Goris[3,*]

[1] Institut de Biochimie et de Biophysique Moléculaire et Cellulaire
UMR8619, Bât 430
Université de Paris-Sud
91405 Orsay Cedex
France

[2] Section of Structural Biology
Institute of Cancer Research
Chester Beatty Laboratories
237 Fulham Road
London, SW3 6JB
United Kingdom

[3] Afdeling Biochemie
Faculteit Geneeskunde
K.U.Leuven
B-3000 Leuven
Belgium

[4] Ecole Polytechnique Fédérale de Lausanne
Laboratoire de Cristallographie
CH-1015 Lausanne
Switzerland

Summary

PTPA, an essential and specific activator of protein phosphatase 2A (PP2A), functions as a peptidyl prolyl isomerase (PPIase). We present here the crystal structures of human PTPA and of the two yeast orthologs (Ypa1 and Ypa2), revealing an all α-helical protein fold that is radically different from other PPIases. The protein is organized into two domains separated by a groove lined by highly conserved residues. To understand the molecular mechanism of PTPA activity, Ypa1 was cocrystallized with a proline-containing PPIase peptide substrate. In the complex, the peptide binds at the interface of a peptide-induced dimer interface. Conserved residues of the interdomain groove contribute to the peptide binding site and dimer interface. Structure-guided mutational studies showed that in vivo PTPA activity is influenced by mutations on the surface of the peptide binding pocket, the same mutations that also influenced the in vitro activation of PP2Ai and PPIase activity.

Introduction

PP2A is one of the major protein serine/threonine phosphatases responsible for regulating the levels of intracellular protein phosphorylation (Janssens and Goris, 2001; Janssens et al., 2005). The enzyme controls diverse activities, including metabolism, DNA replication, transcription, RNA splicing, translation, cell cycle progression, morphogenesis, development, and transformation. Its capacity to regulate these processes is governed by regulatory and targeting subunits and posttranslational modification.

The core PP2A holoenzyme comprises a 36 kDa catalytic subunit ($PP2A_C$) and a 65 kDa HEAT-motif containing scaffolding subunit (PR65/A) (Groves et al., 1999). This core heterodimer ($PP2A_D$) either exists independently (Kremmer et al., 1997) or associates with one of a variety of variable (B) subunits, which confer regulatory and specificity functions (Janssens and Goris, 2001). The three major classes of B subunit (PR55/B, PR61/B′, and PR72/B″) share little sequence similarity, except for two conserved A subunit binding domains (Li and Virshup, 2002). Mechanisms that regulate PP2A include variation in its subunit composition (reviewed in Janssens et al. [2005]), inactivating threonine and tyrosine phosphorylations of its catalytic subunit (Chen et al., 1992; Guo and Damuni, 1993), phosphorylation of PR61/B′ subunits (McCright et al., 1996; Usui et al., 1998), and reversible methylation (Favre et al., 1994) of the $PP2A_C$ C terminus catalyzed by the specific methyltransferase LCMT (PP2A leucine carboxyl methyltransferase) (De Baere et al., 1999; Leulliot et al., 2004) and methylesterase PME-1 (Ogris et al., 1999).

PP2A is also regulated by the action of PTPA, a protein that was originally described for its capacity to stimulate the tyrosyl phosphatase activity of $PP2A_D$ (Cayla et al., 1990). However, recent findings suggest that its physiological function is more likely to reactivate the Ser/Thr phosphatase activity of an inactive form of PP2A ($PP2A_i$) (Longin et al., 2004; Van Hoof et al., 2005; Jordens et al., 2006) that forms a stable complex with PME-1 (Longin et al., 2004). Human PTPA is encoded by a single gene, mapped to chromosome 9q34 (Van Hoof et al., 1995). The transcription gives rise to seven different splice variants, four of which are active (Janssens et al., 2000b). Basal expression of the gene is dependent on the ubiquitous transcription factor Yin Yang 1 (Janssens et al., 1999) and functionally antagonized by p53 (Janssens et al., 2000a).

In budding yeast, PTPA is encoded by two genes, *YPA1* and *YPA2* (also named *RRD1* and *RRD2* for *R*apamycin-*r*esistant *d*eletion). Individual deletion of *YPA1* produces a more severe phenotype than deletion of *YPA2*. Deletion of *YPA1* leads to an aberrant bud morphology, abnormal actin distribution, growth defects, and rapamycin resistance (Van Hoof et al., 2000, 2001; Rempola et al., 2000). Ypa1 and Ypa2 deletions confer rapamycin resistance probably by indirect regulation of TOR, the key component of a nutrient sensing signaling cascade that controls a wide spectrum of growth-related events in response to nutrient availability and growth factor signaling (see Jacinto and Hall [2003] and Zabrocki et al. [2002] for reviews). Whereas Ypa1 has a major role in the G1 phase of the cell cycle (Van Hoof et al., 2000) and also functions in the regulation of the

*Correspondence: jozef.goris@med.kuleuven.be
[5] These authors equally contributed to the work.
[6] Additional correspondence: david.barford@icr.ac.uk
[7] Additional correspondence: herman.van-tilbeurgh@ibbmc.u-psud.fr

G2/M transition (Mitchell and Sprague, 2001), Ypa2 functions in M phase (Van Hoof et al., 2001). Deletion of both genes is lethal (Van Hoof et al., 2000, 2001; Rempola et al., 2000), although this synthetic lethality is suppressed by the "viable" allele (SSD1-v1) of the SSD1 (*s*uppressor of *S*it4 *d*efects) gene (Rempola et al., 2000; Fellner et al., 2003; Kaeberlein et al.,2004), suggesting that Ypa1 and Ypa2 might function in the cell integrity pathway. Loss of PTPA function caused the synthesis of a less stable form of PP2A with an increased protein tyrosine phosphatase-like activity, as assessed by its capacity to dephosphorylate the phosphotyrosine mimetic *p*-nitrophenol phosphate (Fellner et al., 2003). This suggested that PTPA was probably essential for defining the native conformation of PP2A (Fellner et al., 2003). Genetic evidence identified *YPA1* and *YPA2* as positive regulators of PP2A (Rempola et al., 2000; Van Hoof et al., 2000) and PP2A-related phosphatases such as Sit4 (Mitchell and Sprague, 2001, Douville et al.,2004), implicated in the regulation of the TOR pathway (Van Hoof et al., 2005). Recent studies revealed that Ypa1 physically interacts with the PP2A-like phosphatases Pph3, Sit4, and Ppg, whereas Ypa2 binds to Pph21 and Pph22, the yeast homologs of PP2A. This latter interaction is promoted by Ypa1 (Van Hoof et al., 2005). Moreover, the different PP2A-like phosphatases in yeast (Pph21, Pph22, Pph3, Sit4, and Ppg) can exist as inactive conformers that can be activated by Ypa1 or Ypa2 (Van Hoof et al., 2005).

The activation of PP2A by PTPA, Ypa1, or Ypa2 is dependent on ATP or a hydrolysable ATP analog with Mg^{2+} (Cayla et al., 1990; Van Hoof et al., 1998). However, a kinase activity could not be demonstrated, consistent with the absence of detectable kinase sequence signature motifs. The mechanism of activation remained elusive until the recent identification of PTPA/Ypa1/Ypa2 as a peptidyl-prolyl *cis*/*trans* isomerase (PPIase) (Jordens et al., 2006). Moreover, we were able to propose the conserved Pro190 in $PP2A_C$ as the target for an isomerization reaction. This Pro190 is not only conserved during evolution in the different species, but also the sequence of the loop structure is also conserved in all PP2A-like phosphatases, suggesting that the activation might be a very specific mechanism.

In addition to their role in PP2A activation, stable ternary complexes of Tap42-Ypa1-Sit4 and Tap42-Ypa2-$PP2A_C$ have been observed (Van Hoof et al., 2005; Zheng and Jiang, 2005). Yeast Tap42 and the mammalian equivalent α4 are proteins that interact directly with $PP2A_C$ independent of the PR65/A subunit and are known to be important players in the TOR signaling pathway (Di Como and Arndt, 1996; Murata et al., 1997) (see Jacinto and Hall [2003] for a review). The human homolog of Tap42, α4, is also described as an inhibitor of apoptosis (Kong et al., 2004). A partially overlapping role for Ypa1 and Tap42-associated PP2A or PP2A-like phosphatases is suggested from the finding that overexpression of Tap42 suppresses the rapamycin resistance of the Ypa1 deletion strain (Van Hoof et al., 2005). However, the mechanisms by which Tap42/Ypa/PP2A complexes interfere with the TOR signaling pathway are still largely unknown.

In an effort to understand the mechanism of PTPA action at the molecular level, we determined the crystal structures of both yeast Ypa1 and Ypa2 as well as human PTPA. The three structures are very similar, revealing an all α-helical protein fold where highly conserved residues line a groove between two lobes of the molecule. In order to understand the basis of PTPA action, we cocrystallized Ypa1 with a peptide active in the prolyl-isomerase reaction. The complex provides a definition of the peptide binding site and reveals that a group of conserved residues were involved in dimerization of the protein. Structure-guided mutational studies showed that in vivo PTPA activity is influenced by mutations on the surface of the peptide binding pocket, the same amino acids that also influenced the in vitro activation of PP2Ai and PPIase activity.

Results

Structure Determination

Because full-length Ypa1, Ypa2, and hPTPA (isoform α) proteins failed to crystallize, we decided to construct truncated versions of these proteins by removing nonstructured regions identified by sequence analysis and limited proteolysis. These regions correspond to the C-terminal region of Ypa1 and Ypa2 and the N-terminal region of hPTPA (Figure 1). The crystallized proteins, named Ypa1Δ, Ypa2Δ, and hPTPAΔ hereafter, comprise regions 1–320, 1–304, and 20–323, respectively. The structure of Ypa2Δ was solved by single anomalous diffraction using selenomethionine-substituted crystals. The radiation damage on the selenium atoms was modeled and used in a "continuous" radiation damage-induced phasing (RIP) scheme implemented in SHARP in order to obtain interpretable electron density maps (see Experimental Procedures) (Schiltz et al., 2004). The resulting maps enabled the two protein chains present in the asymmetric unit to be modeled. The structure of Ypa1Δ was solved by molecular replacement using a model derived from the Ypa2Δ structure. Application of density modification reflecting the 2-fold symmetry of the two monomers present in the asymmetric unit was necessary to yield a high-quality map. Despite the presence of noncrystallographic translational symmetry and severe anisotropy of the diffraction data, the structure of Ypa1Δ in complex with the peptide substrate was solved by molecular replacement using the native Ypa1Δ structure as a search model. Four copies of Ypa1Δ are present in the asymmetric unit. In contrast to the monomeric assembly of Ypa1Δ in the absence of peptide, the protein formed two independent dimers in the asymmetric unit when in complex with the peptide substrate (see below). The structure of hPTPAΔ was solved independently by single anomalous diffraction (SAD) using selenomethionine-derived crystals. hPTPAΔ data collection did not undergo radiation damage, and initial SAD-derived phases resulted in a readily interpretable high-resolution electron density map. There is one hPTPAΔ molecule per asymmetric unit, and the structure was refined to 1.5 Å resolution. Data collection and refinement statistics are reported in Table 1.

PTPA Represents an All Helical PPIase Architecture

The Ypa1Δ, Ypa2Δ, and hPTPAΔ proteins share on average 38% sequence identity and therefore possess an identical fold, belonging to the all α class (topology in

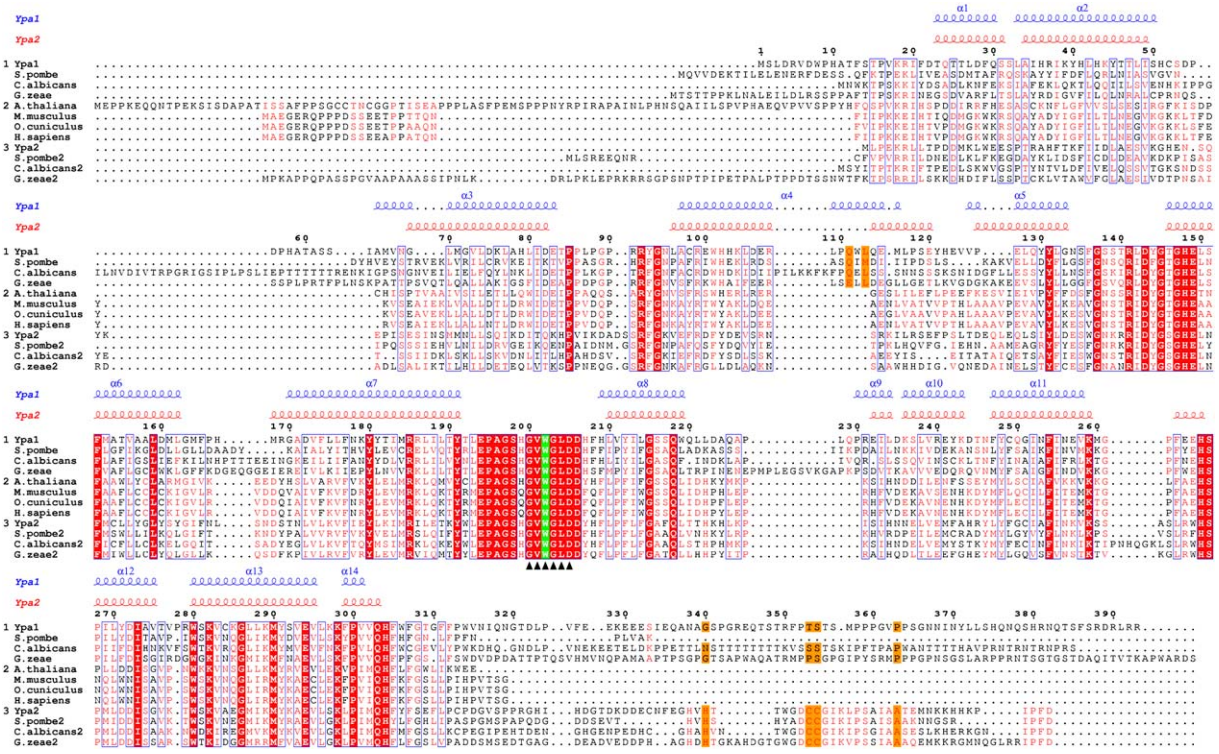

Figure 1. Multiple Sequence Alignment of PTPA Proteins

Alignment was performed with CLUSTAL W (Thompson et al., 1994) and represented with ESPRIPT (Gouet et al., 1999). The proteins have been separated in three families: Ypa1-like (*S. cerevisiae*, *S. pombe*, *C. albicans*, and *G. zeae*), hPTPA-like (*A. thaliana*, *M. musculus*, *O. cuniculus*, and *H. sapiens*), and Ypa2-like (*S. cerevisiae*, *S. pombe*, *C. albicans*, and *G. zeae*). Secondary structure elements as extracted from the present crystal structures are superposed. The amino acids deleted in the inactive mutant of *O. cuniculus* are indicated by black triangles. The absolutely conserved tryptophan involved in stacking with the proline ring is highlighted in green.

Figure 2A). The PTPA fold is composed of 14 α helices, organized into two discrete domains each of ~25 Å in diameter. The interface of the two domains defines a prominent groove. Helices α3–α7 (shades of blue in Figure 2A) stack by extensive hydrophobic interactions and form a well-defined five helical bundle. This helical bundle defines a structural domain of the PTPA fold (domain A) and displays superficial similarity to the cyclin box fold. However, both the topology and relative disposition of the five antiparallel helices of domain A of PTPA differ from the cyclin box structure (Figure 3). Moreover, the narrow conserved groove at the domain interface is analogous to the peptide binding groove within the N-terminal cyclin box folds of cyclin A (Brown et al., 1999) and retinoblastoma (Lee et al., 1998). The second domain (domain B, shades of red and purple in Figure 2A) contains helices α8–α13, with α8 and α11 packing along sides α6 and α7 of domain A. Domain B shares a similar topology to domain A, although in contrast to domain A where the average length of the helices is six to seven turns, the α helices of domain B comprise only two to three turns. The N-terminal helices α1 and α2 (shades of green in Figure 2) run along the lengths of both domains A and B, whereas the C-terminal helix α14 stacks on the α1 helix.

The overall structures of Ypa1Δ, Ypa2Δ, and hPTPAΔ are essentially identical with an average root-mean-square deviation (rmsd) of 1.1 Å (Figure 2B). All α helices are perfectly superimposable in the three proteins, and the largest differences between the three homologs are confined to conformational changes of the α2-α3 and α8-α9 loops. For some copies in the asymmetric units of Ypa1Δ and Ypa2Δ, a few residues of the α3-α4 and α7-α8 loops are not visible in the electron density, suggesting that these loops are flexible. A search for structural homologs with full-length or with separate domains of PTPA did not retrieve significant matches. The Ypa1Δ, Ypa2Δ, and hPTPAΔ structures therefore did not initially provide clear insights into their biochemical function. Sequence alignment of PTPA homologs shows that they contain an almost absolutely conserved α7-α8 loop (Figure 1). This loop connects domain A and B and lines the groove at the interface of the two domains (Figures 2C and 2D, see also Figure S4 available in the Supplemental Data with this article online). The other residues lining this groove are also mostly conserved and belong to the α3-α4, α5-α6, and α11-α12 loops and to α13 helix (Figure 2C and Figure S4). This highly conserved groove, confined between the two domains, would seem to be an ideal candidate for harboring the biochemical function of PTPA proteins. However, no canonical ligand binding, metal binding, or putative catalytic site could be identified in this groove.

Prolyl Containing Peptides Bind to a Conserved Region at a Peptide-Induced Dimer Interface

The biochemical function of PTPA proteins was recently identified as a peptidyl-proline isomerase activity by the

Table 1. Data Collection and Refinement Statistics

Protein	hPTPA (Native)	Yap2Δ (SeMet pk)	Yap1Δ	Yap1Δ+ppi-Peptide
Space group	$P2_12_12_1$	$C222_1$	$P2_12_12_1$	$P6_5$
Unit-cell parameters: a, b, c (Å)	48.2 70.4 95.5	157.9 171.0 53.7	53.1 94.2 139.8	86.9 86.9 410.6
Resolution (Å)	1.50 (1.58–1.50)	2.8 (2.87–2.8)	2.6 (2.74–2.6)	2.8 (2.95–2.80)
Total number of reflections	311,889 (44,972)	176,445 (13,572)	133,991 (18,579)	165,026 (24,003)
Total of unique reflections	52,866 (7599)	19,075 (1938)	21,334 (3181)	42,938 (6228)
Multiplicity	5.9 (5.0)	9.3 (7.1)	6.3 (5.8)	3.8 (3.8)
R_{merge}[a]	0.091 (0.296)	0.192 (0.55)	0.139 (0.429)	0.198 (0.647)
$I/\sigma(I)$	13.7 (5.9)	11.5 (2.6)	11.9 (3.7)	5.7 (2.0)
Overall completeness (%)	99.9 (100)	91.4 (95.2)	95.5 (100.0)	99.9 (99.9)
R/R_{free} (%)[b]	20.2/22.1	20.2/27.3	21.4/29.0	21.6/29.2
Rmsd bonds (Å)	0.009	0.022	0.018	0.024
Rmsd angles (°)	1.21	2.26	1.84	2.48
Ramachandran plot (%)				
Most favored	93.6	85.7	90.5	82.4
Allowed	6.4	14.3	9.5	17.6

[a] $R_{merge} = \Sigma_h\Sigma_i \mid I_{hi} - \langle I_h \rangle \mid / \Sigma_h\Sigma_i I_{hi}$, where I_{hi} is the *i*th observation of the reflection h, whereas $\langle I_h \rangle$ is the mean intensity of reflection h.
[b] $R_{factor} = \Sigma \| F_o \| - \| F_c \| / \| F_o \|$. R_{free} was calculated with a small fraction (5%) of randomly selected reflections.

use of NMR spectroscopic and biochemical assays (Jordens et al., 2006). Conventional peptidyl-proline isomerases belong to three distinct families (cyclophilins, FKBPs, and parvulins) whose structure and mechanism have been extensively studied. Their folds are all characterized by a central β sheet. Clearly, PTPA is structurally unrelated to any of these PPIases. Therefore, in order to elucidate the structural basis of PPIase activity of PTPA proteins, we performed cocrystallization trials with all the PTPA homologs using different peptide mimics. These short peptides (four to ten residues), synthesized with $PP2A_C$ sequences centered on proline residues, had previously been tested in the PPIase reaction.

Of all the different trials performed, using all three PTPA homologs, only cocrystallization of Ypa1Δ with LQEVPHEGPMCDL, the PP2A peptide active in PPIase reaction, and succinyl-AlaAlaProLys-paranitroanilide (suc-AAPK-pNa), the standard substrate used in the biochemical activity assay for PPIases, were successful (in the same crystallization conditions). Only crystals with suc-AAPK-pNa gave sufficient diffraction to solve the structure. The structure of the complex was solved by molecular replacement using the native Ypa1 structure as a model and unexpectedly revealed two dimers in the asymmetric unit. The dimerization mode of Ypa1Δ is a head-to-head dimer with proper 2-fold symmetry (Figures 4A and 4B).

Dimer formation is achieved by interactions of the α7-α8 and α3-α4 loops onto the opposing α7-α8 and α3-α4 loops, respectively, and of the α5-α6 loop onto the α11-α12 loop. Dimerization involves ~24 residues and buries 1100 $Å^2$ of accessible surface mainly by hydrophobic interactions. Two hydrogen bonds (Ser198-Val201) and four salt bridges (Glu265-Arg141 and Glu194-Arg92) are formed across the complex interface. Structural rearrangements are mainly localized to the central α7-α8 loop, which in the native Ypa1Δ is partially unstructured.

Analytical ultracentrifugation demonstrates the presence of a monomer/dimer equilibrium in solution, but quantification of these experiments is hampered by precipitation of the protein in the monomeric state. Preliminary ultracentrifugation experiments of sedimentation equilibrium revealed aggregation of native Ypa1 and Ypa1Δ in the first hours and the propensity of the ligand succinate-AAPKpNA to slow down this aggregation (data not shown). Apparent sedimentation coefficients were calculated from early profiles of sedimentation velocity experiments at one concentration with and without ligand for both native Ypa1 and Ypa1Δ (Figure S1); s values were not extrapolated at zero protein concentration. Despite high residuals and broad c(s) peaks protein aggregation, we found for both proteins species s values compatible with monomers in the absence of ligand, and monomers and dimers in the presence of ligand.

At the outset of the crystallographic refinement, clear unassigned electron density was visible in two pockets of the Ypa1Δ dimer for both copies in the asymmetric unit. This density could be unambiguously modeled by the suc-AAPK-pNa peptide (Figure 4A). Apart from the succinate residue, the entire peptide, including the pNa chromophore, is well defined in the structure. The presence of the chromophore and the lysine residue clearly defines the direction of the peptide chain in the electron density.

Two copies of the suc-AAPK-pNa peptide are bound in two symmetrical pockets created at the Ypa1-dimer interface. This pocket is lined with residues belonging to α12, α13, and the α7-α8 loop from one monomer, and α1, the N terminus of α14, from the other monomer (Figure 4B). The peptide binds by extensive hydrophobic interactions (Figure S2). One hydrogen bond is formed by the backbone oxygen of the second alanine of the peptide and the backbone nitrogen of Phe299. The absolutely conserved Lys298, which makes a salt bridge to Glu294 in the same protein chain, is located on average 4 Å from the succinate group, probably leading to favorable electrostatic interactions. Asp272 makes a salt bridge with the lysine present in the peptide, but this aspartate is replaced by asparagine in some organisms (Figure 1). Catalytic PPIase assays using NMR performed with peptide substrates that do not contain a charged residue after the Pro show that this

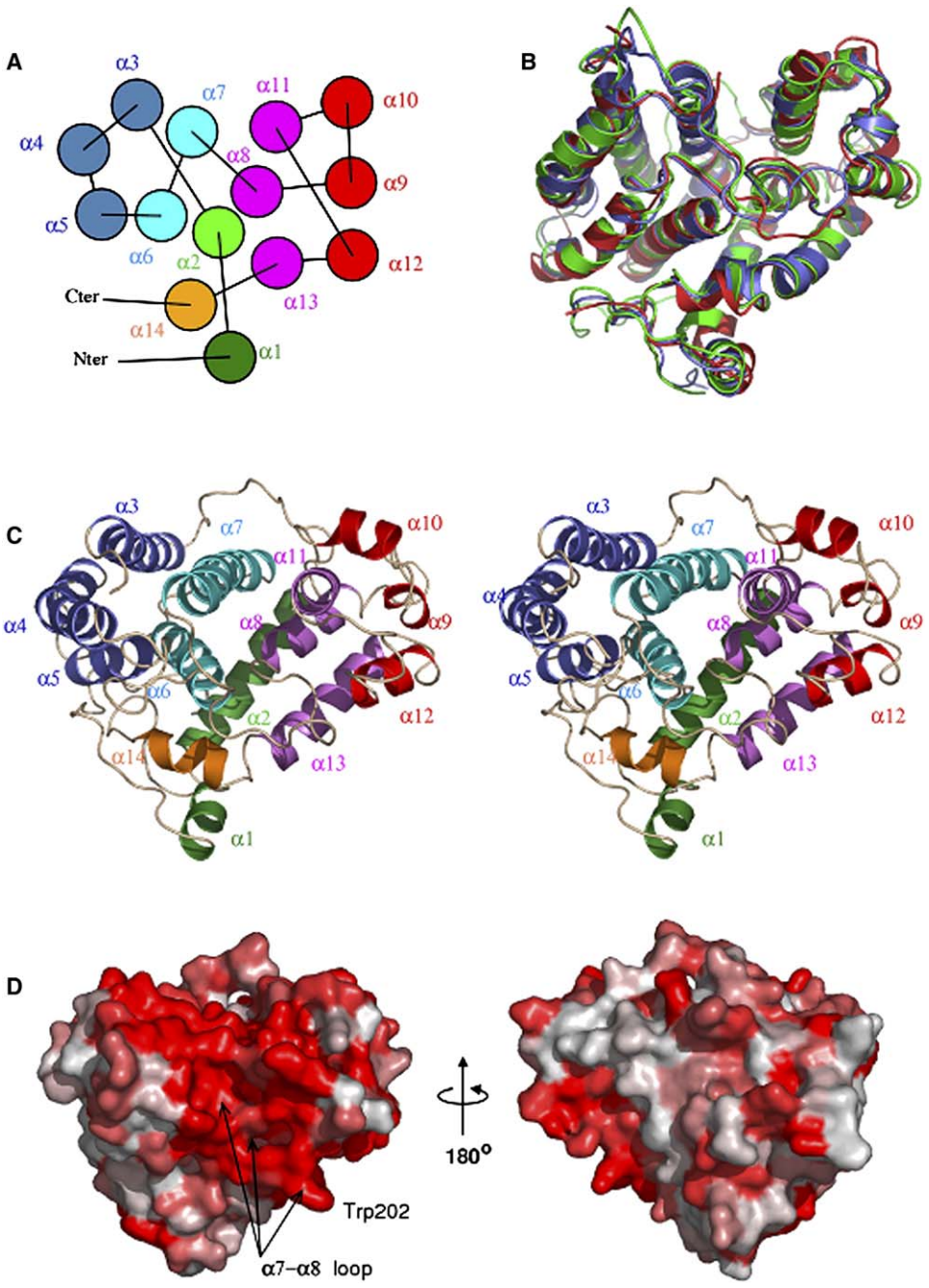

Figure 2. Structure of PTPA Homologs

(A) Topology of the PTPA fold. The bimodular structure is formed by domain A (helices 3–7) and domain B (helices 8–13).

(B) Structural superposition of hPTPAΔ (blue), Ypa1Δ (green), and Ypa2Δ (red), in about the same orientation as (C).

(C) Stereo cartoon representation of the Ypa1Δ monomer. The helices are colored with the same color code as (A).

(D) Surface representation of the Ypa1Δ monomer. The surface is color coded in increasing shades of red representing conservation of the surface residue. The left panel has the same orientation as (C), whereas in the right panel, the Ypa1Δ monomer is rotated over 180°.

salt bridge is not required for PPIase activity (Jordens et al., 2006). The most prominent feature of the interaction is the hydrophobic sandwich interaction of the suc-AAPK-pNa peptide proline with the side chains of the absolutely conserved Trp202 and a minor contact to Pro268 (Asn268 in group 2 PTPAs, see Figure 1). Trp202 is itself stacked onto His199 of the opposing monomer. The peptide is bound in a *trans* conformation with Phi/Psi angles of −60/150° (Figure 4C).

Conserved Residues Are Required for PP2A Activating and PPIase Activity of Ypa1 Mutants

In previous investigations, we showed that the conserved region $_{200}$GVWGLD$_{205}$ of PTPA (Ypa1 numbering) is essential for both the activation of the tyrosyl phosphatase activity of PP2A$_D$ as well as for the activation of PP2A$_i$ and the PPIase activity (Jordens et al., 2006; Van Hoof et al., 1998). Deletion of this region diminished PTPA activity. This absolutely conserved region,

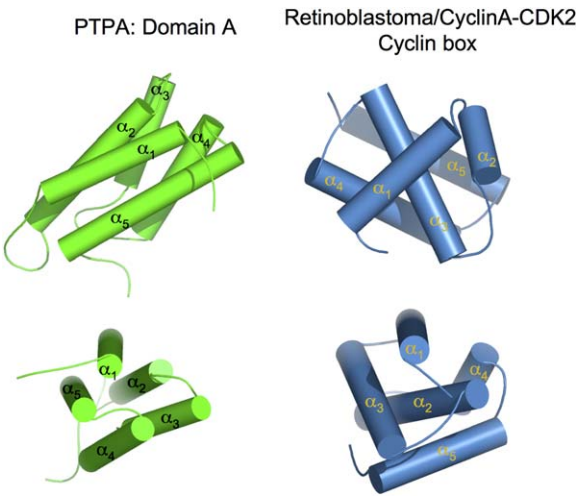

Figure 3. Comparison of PTPA A Domain and the Cyclin A/Retinoblastoma Fold

Comparison of the helical fold of domain A of PTPA with the cyclin box fold of cyclin A. Both domains feature an antiparallel five α-helical bundle, although the topology of the two domains differs.

situated in the α7-α8 loop and linking the two domains of the protein, corresponds to the peptide binding site (residue numbers highlighted in red in Figure 4B). The structure of this mutant from *O. cuniculus* was probed by CD spectroscopy to ensure that its loss of activity was only due to the deleted binding site and not to disruption of the overall structure. The CD spectra of *O. cuniculus* PTPAΔ($_{200}$GVWGLD$_{205}$) indicated no loss of α-helical structure compared to wild-type PTPA of the same species (Figure S3) or to wild-type Ypa1Δ (data not shown).

We further explored the importance of individual amino acids in this sequence by testing the PP2A$_i$ activation and PPIase activities of the following point mutations: Trp202Gly, Gly203Phe, Asp205Gly, and Asp206Gly (Table 2). The Asp205Gly mutation caused similar changes in both PP2A activating and PPIase activity as compared to the $_{200}$GVWGLD$_{205}$ deletion mutant (Jordens et al. [2006] and Table 2). The Asp206Gly mutant is almost completely inactive in the activation and 50% less active in the PPIase reaction. The Trp202Gly mutant and to a lesser extent Gly203Phe show a low specific activity in the activation reaction, although they were active in the protease-based PPIase assay. Because the Trp202Gly mutant was expected to be inactive as a PPIase, we sought independent evidence for the PPIase activity of some mutants by dynamic protein NMR spectroscopy using the band-shape analysis technique (Hübner et al.,1991) as applied in Jordens et al. (2006), with the Pro190-containing, PP2A$_C$-derived peptide ^{186}LQEVPHEGPMCDL^{198} as substrate. By using this method and substrate, the Trp202Gly mutant was inactive as a PPIase, as was the Asp205Gly mutant (Figure 5, compare with wild-type). A possible reason for this apparent discrepancy between both methods is explained in the Discussion.

We further tested the effect of mutations introduced in most of the amino acids lining the groove between domains A and B in the dimer interface region (Arg92, Lys259, and His266) (see Figure S4). As a control, we tested mutants of residues that are part of a conserved surface patch distinct from the peptide binding site and dimerization interface (Arg185 and Phe254). Although not as drastic as the Trp202, Asp205, or Asp206 point mutants, the interface mutations at residues Arg92, Lys259, and His266 slightly impair the capability of PTPA/Ypa1 to activate PP2A$_i$, whereas the other mutants (Arg185 and Phe254) hardly influenced the specific activity as activator. None of the mutants significantly influenced the PPIase activity, except for Asp205 and Asp206, which diminished activity substantially. These last mutants certainly hinder the peptide binding by disrupting the protein dimer interface.

As a positive control, Leu270Ala and Val277Ala mutants, located near the peptide groove without being directly involved in binding, were designed to test for destabilizing the overall structure of PTPA. The Val277Ala was found to be about 5-fold less active as an activator of PP2A$_i$ in comparison with wild-type Ypa1, whereas we found only a very low expression of soluble Leu270Ala mutant and could therefore neither measure activity changes nor PPIase activity.

Mutations of the Dimer Interface and Peptide Binding Pocket Disrupt In Vivo Activity

We designed an assay for the effects of the mutations of Ypa1 on a known physiologic effect of Ypa1 in vivo. Deletion of Ypa1 in W303-1Aα yeast strains confers rapamycin resistance (Van Hoof et al., 2000; Rempola et al., 2000). Reintroduction of wild-type Ypa1 rescues this phenotype. We reasoned that by reintroduction of a nonfunctional Ypa1, the strains would still grow on rapamycin. This was indeed the case for the Asp205Gly, Asp206Gly, Leu270Ala, and Val277Ala mutants and somewhat less for the Trp202Gly, Gly203Phe, and Lys259Gly mutants, whereas none of the other Ypa1 deletion strains transfected with mutant Ypa1 showed any growth after 5 days of incubation (the control Arg185Gly mutant is shown as an example) (Table 2 and Figure S6).

Discussion

The activity of PP2A is subject to complex regulation. The biochemical mode of action is well documented for a few of its regulators (methyltransferase [De Baere et al., 1999] and methyl esterase [Favre et al., 1994]), whereas for others the activation mechanism remains more elusive. PTPA is an activator of the inactive form of PP2A, whose biochemical function was unknown until recently. The activation of PP2A$_i$ by PTPA, Ypa1, or Ypa2 is dependent on the presence of MgATP or a hydrolysable ATP analog. Surprisingly, PTPA does not possess kinase activity, but ATP/Mg^{2+} stimulates the recently discovered prolyl *cis/trans* isomerase activity of PTPA. PTPA PPIase activity could be clearly demonstrated with a biochemical assay that uses a generic peptide and was comparable to activities from well-characterized PPIases such as cyclophilin and FKBP (Jordens et al., 2006). Among the 14 proline residues of PP2A represented in synthetic peptides, only one reacted in the presence of PTPA and ATP/Mg^{2+}. Through the present crystal structures of PTPA, Ypa1, and Ypa2, the molecular basis of their action can be defined further.

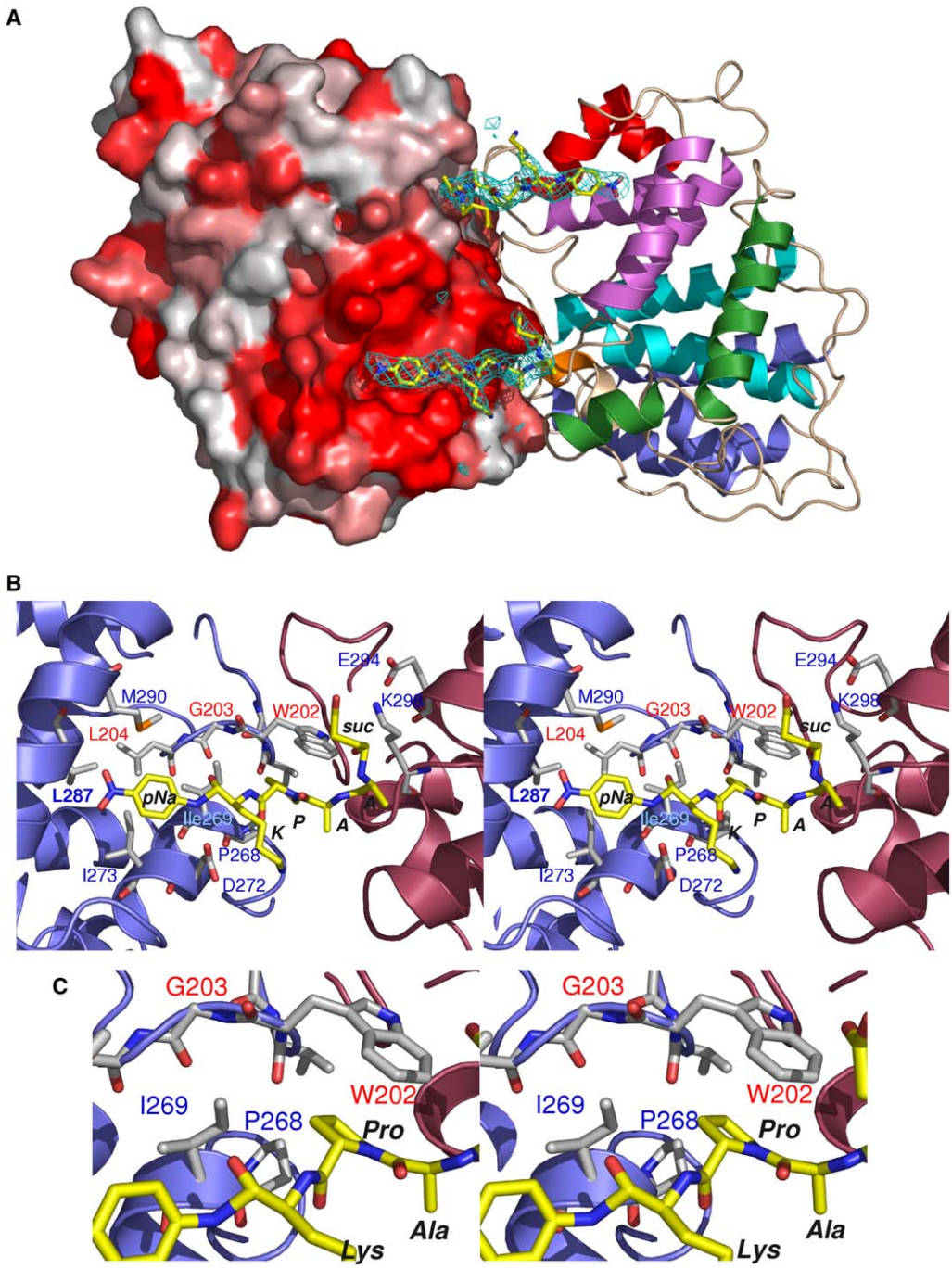

Figure 4. Structure of Ypa1Δ in Complex with the PPIase Substrate suc-AAPK-pNa

(A) Binding of the suc-AAPK-pNa peptide involves dimerization of Ypa1Δ. One monomer has the same color code as Figures 2A and 2B, the other is represented in surface colored as in Figure 2D. The $F_o - F_c$ electron density contoured at 3σ is shown for the PPIase peptides.

(B) Stereo view of the peptide binding pocket. The two monomers are colored red and blue. The residues of the protein in proximity to the peptide are labeled. The residues labeled in red correspond to the region deleted in the inactive mutant from *O. cuniculus*.

(C) Close-up view of the stacking interaction of Trp202 and the peptide proline. Peptide residues are labeled in bold.

PTPA Proteins Define a Fold

PTPA, Ypa1, and Ypa2 are all bilobal proteins, containing exclusively α helices. Therefore, the apo protein structures alone provided relatively few insights into their mechanisms by comparison to known protein structures. The majority of conserved surface residues cluster into a groove situated between the two lobes lined by well-conserved charged residues (Figure 2D). The structure of a complex between Ypa1 and the peptide used for the biochemical isomerase assay yielded crucial information to define the molecular mechanism of PTPA. First, it showed that peptide binding induces dimer formation, and second, it showed that the peptide binds into a hydrophobic groove, juxtaposed to the dimer interface but devoid of a clear set of possible catalytic residues. Analysis of the dimer interface against

Table 2. Activity of Ypa1 Mutants In Vitro and In Vivo

	Position	Activator U/mg	PPIase k_{obs} s^{-1} × 10^{-2}	PPIAse NMR Based	Growth on Rapamycin
Wt		200 ± 10	7 ± 1	Yes	–
Peptide binding interface					
W202G	α7-α8	31 ± 8*	6 ± 1	No	++
G203F	α7-α8	120 ± 20*	7.5 ± 0.8	No	+
P268A	α12	210 ± 10	NM	Yes	–
Dimer interface					
R 92G	α3-α4	160 ± 40	7.2 ± 0.9	–	–
D205G	α7-α8	4.9 ± 0.8*	2.1 ± 0.3*	No	+++
D206G	α7-α8	40 ± 1*	3.4 ± 0.6*	–	+++
K259G	α11	160 ± 20	6.8 ± 0.4	–	+
H266G	α11-α12	150 ± 10	7.4 ± 0.7	–	–
Other conserved surface patch					
R185G	α7	200 ± 80	6.5 ± 0.6	–	–
F254G	α11	190 ± 20	7 ± 1	–	–
Structure destabilizing					
L270A	α12	NM	NM	–	++
V277A	α12-α13	40 ± 2*	1.9 ± .1*	–	+++

Activity of the different Ypa1 mutants was measured by activating PP2Ai. PPIase activity of the different Ypa1 mutants was measured with the protease-assisted method and suc-AAPK-pNA as substrate or with the ^{1}H-NMR-based method and the PP2A-derived peptide. Details of the different methods can be found in the Supplemental Data. All quantitative experiments were measured in triplicate. The mean values are given ± standard deviation. The significance of the difference (p value < 0.05) between the mutants and wild-type Ypa1 measurements is indicated by an asterisk (*). NM means not measured. A minus sign (–) in the "PPIase NMR Based" column also means not measured.

sequence data shows that dimer formation involves highly conserved surface regions.

Ypa1 and Ypa2 physically interact with different phosphatases in vitro. Based on sequence conservation, it is possible to group the PTPA proteins into three subfamilies: PTPAs from higher eukaryotes and from the two paralogous subfamilies in yeast (Figure 1). We presently solved the structures of one member of each subfamily and demonstrated structural conservation at the putative catalytic site. The variable residues defining the three families are therefore probably involved in fine tuning of the binding specificity of the PTPA protein to PP2Ac and other PP2A-like phosphatases, and possibly to the other PP2A regulatory subunits (Tpd3 and Tap42 in yeast).

PTPA Is a Peptidyl-Proline *cis*/*trans* Isomerase with an Unknown Catalytic Mechanism

The PTPA fold is radically different from that of the conventional prolyl *cis*/*trans* isomerases. Currently known peptidyl-proline isomerases belong to three families: cyclophilins, FKBPs, and parvulins. The catalytic mechanism of these PPIases is still unclear, despite the wealth of structural data relating to the three different PPIase families and of their complexes with inhibitors, peptides, or proteins (for review see Fanghanel and Fischer [2004]). It also remains unclear if the catalytic pathway of the enzymes of the three families is related or if they adopt different strategies for their enzymatic activity.

A number of catalytic mechanisms have been proposed for *cis*/*trans* isomerases, but the possibility of a nucleophilic attack from a side chain in the PPIase active site has been excluded. The acceleration of the *cis*/*trans* isomerization of prolyl bonds involves the reduction of the double bond character of the C-N bond, and hydrogen bonding of a catalytic site arginine to the amide oxygen immediately C-terminal to the prolyl residue also seems to play a role. PPIases bind and stabilize a transition state that is characterized by partial rotation around the C-N bond, and the energetic cost for this is compensated by favorable interactions between enzyme and substrate transition state (Harrison and

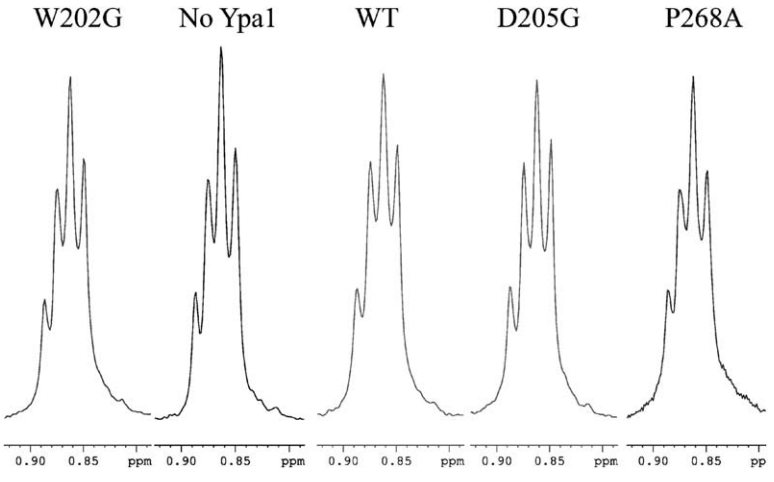

Figure 5. ^{1}H-NMR Spectra of the PP2A-Derived Peptide

Shown is a region of a one-dimensional NMR proton spectrum with signals from methyl groups in the $_{186}$LQEVPHEGPMCDL$_{198}$ peptide in the presence or absence of 5 μM Ypa1 or the Ypa1-indicated mutants in the conditions described in the Supplemental Data.

Stein, 1990). Hydrophobic interactions further anchor the proline in a hydrophobic pocket. The proline bond is therefore distorted by electrostatic and/or geometrical interactions toward the transition state.

As judged from the Ypa1 peptide complex, no arginine or any other charged side chain is in an appropriate position to form a hydrogen bond with the proline peptide bond. However, a "conformational distortion mechanism," where catalysis is performed by destabilizing the substrate by using the binding energy of the peptide without the need for specific hydrogen bonds, is still possible. At the present resolution of the structure of the Ypa1 complex, we are unable to detect a distortion of the imide bond of the substrate peptide. Recognition of residues surrounding the substrate proline by electrostatic or hydrogen bonding also undoubtedly contributes to the efficiency of binding and/or catalysis. The hypothetical involvement of activated water molecules in some PPIases leads to more complicated catalytic mechanisms. The presence of metal ions might also play a role in the efficiency of catalysis.

Interplay of PP2A Activating and PPIase Activities

In the absence of obvious polar or charged candidate residues that could play a role in catalysis, we tested the contribution of hydrophobic residues to binding and activity. A drastic deletion of the totally conserved $_{200}$GVWGLD$_{205}$ peptide yields a PTPA variant that is inactive in both the PPIase and the PP2Ai activation reactions (Jordens et al., 2006). This mutation completely removes the peptide binding site in the α7-α8 loop (Figure 4B) without affecting the global structure of the protein in solution (Figure S3). Within this loop, the absolutely conserved Trp202 (colored in green in Figure 1) certainly makes the most prominent contact by stacking with the proline (Figure 4C). Consistent with this observation, the PP2A activation and in vivo activity are severely reduced in Trp202 mutants. The Gly203Phe mutation, which introduces a bulky side chain in the peptide binding site, has only a mild effect in the PP2Ai activation reaction, whereas the Asp205Gly and Asp206Gly mutations in the dimerization site had drastic effects, and mutations in a distinct conserved patch had no effect. Surprisingly, only the Asp205 and Asp206 point mutants, which disrupt the dimerization site, resulted in a reduction of in vitro PPIase activity. The loss of in vivo activity despite the persistence of wild-type PPIase for some mutants could reflect a limitation of the protease-based PPIase assay, which might be less sensitive to mutations when measured on short peptides as opposed to longer peptides or the full-length protein. This can be seen when PPIase is measured by the ^{1}H-NMR "peak broadening" technique: in this case, neither the D205G mutant nor the W202G mutant could isomerase Pro190 in the context of the PP2A$_C$-derived peptide ^{186}LQEVPHEGPMCDL^{198} as opposed to wild-type (see Figure 5). Unfortunately, in the protease-assisted PPIase activity measurements, the chromophore or fluorophore is obligatory positioned next to the protease cleavage site following the Pro, whereas the ^{1}H-NMR-based PPIase does not have these limitations although it is only qualitative and not quantitative. Therefore, although the correlation of PPIase-in vitro activation and in vivo activity is rather strict, it does not exclude the possibility that another function besides PPIase is necessary for the full activation of PP2A in vivo. A precedent is found for cyclophilins, whose well-characterized prolyl isomerase activity is distinct to its role in inhibition of protein phosphatase 2B (calcineurin) (Jin and Harrison, 2002).

ATP Binding of PTPA

Both PP2A activating and prolyl isomerase activity increase significantly in the presence of ATP/Mg^{2+}, although no turnover of the nucleotide is required. No canonical ATP binding site was identified in the Ypa1 peptide complex, and we did not observe nucleotide bound to hPTPAΔ when cocrystallized with either 10 mM ATP/Mg^{2+} or AMP-PNP/Mg^{2+}. This is consistent with the very low binding affinity expected for ATP. Therefore, the activating effect of ATP/Mg^{2+} could not be structurally defined. Because the truncated versions of PTPA, Ypa1, and Ypa2, used in this study for crystallization, can still activate PP2A$_i$ in a reaction that is dependent on MgATP (data not shown), these N- or C-terminal regions are not involved in the binding of the cofactor. Very recently, it was shown that a conserved proline in the ATPase domain of the Hsc70 chaperone assumed alternative conformations in response to ATP binding and hydrolysis (Vogel et al., 2006), and this conformational change was important for function. Although ATP hydrolysis is not observed in the case of the activation by PTPA, this provides us with a paradigm for the function of PTPA: the "proline switch" would be in the PP2A catalytic subunit, and the action of PTPA, with the ATP cofactor, would be to catalyze the conversion of PP2Ac from the inactive to the active conformation.

Some authors have assigned a chaperone-like function to PTPA, required during the synthesis of PP2A that facilitates incorporation of the required divalent cations into the phosphatase catalytic site (Fellner et al., 2003). However, the structural analysis of PTPA is not consistent with a direct role as a metal-loading protein, because PTPA lacks obvious metal binding sites. Moreover, incubating human PTPA crystals with a variety of divalent cations at high concentrations (e.g., 20–50 mM samarium, zinc, nickel, and manganese) did not reveal the presence of protein bound metals. Finally proton-induced X-ray emission experiments also failed to demonstrate the presence of metal ions associated with PTPA (G.V and D.B., unpublished data). These data suggest that the ability of PTPA to enhance the correct metal coordination at the catalytic site of PP2A results indirectly from its capacity to facilitate the correct native conformation of the PP2A catalytic subunit.

In conclusion, the structures of PTPA, Ypa1, Ypa2, and the Ypa1/peptide complex, combined with previous and recent functional studies, have allowed a much better understanding of the mechanism of action of this PP2A activator. Cocrystallization with a model peptide revealed a new class of prolyl isomerases and defines the molecular basis for recognition of a PP2A substrate. Structure-based mutational studies demonstrated clear links between PTPA in vivo activity, PP2A activation of PTPA, and disruption of the peptide binding and dimerization interface. It has been recognized over the previous few years that local structural rearrangements induced by peptidyl isomerization can serve as molecular

switches (for review see Andreotti [2003]). Further insight into this mechanism for PP2Ai activation will require structure determination of the different conformational states of the phosphatase.

Experimental Procedures

Cloning, Expression, Purification, and Labeling

Ypa1 truncated at residue 320 and Ypa2 truncated at residue 304 were amplified by PCR using genomic DNA of *S. cerevisiae* strain S288C as a template. An additional sequence coding for a 6 histidine tag was introduced at the 3′ end of the gene during amplification. The PCR product was then cloned into a derivative of pET9 vector. Expression was done at 15°C overnight with the transformed *E. coli* Gold (DE3) strain. The His-tagged protein was purified on a Ni-NTA column (Qiagen Inc.) followed by a gel filtration.

Human PTPA (residues 20–323) was amplified by PCR and cloned into the NdeI and BamHI sites of a modified version of pET-17b (Novagen) incorporating an N-terminal His_6 tag and an intervening Prescission protease (Amersham) recognition site. Expression of PTPA was performed at 16°C overnight in *Escherichia coli* strain B834 (DE_3). PTPA was purified via Talon-affinity chromatography, PreScission cleavage, and gel filtration. For crystallization, the protein was eluted in 5 mM HEPES (pH 7.0), 50 mM NaCl, and 3 mM DTT. Selenomethionine-substituted PTPA and Ypa2 were produced and purified as the native protein.

Crystallization, Data Collection, Structure Solution, and Refinement

The crystallization, data collection, structure determination, and refinement statistics for hPTPAΔ, Ypa1Δ, Ypa2Δ, and the Ypa1Δ/peptide complex by X-ray crystallography (Table 1) together with experimental details are detailed in the Supplemental Data. Only the radiation damage-induced phasing is described below.

The structure of Ypa2Δ was solved by SAD aided by radiation damage-induced phasing using data to 2.80 Å resolution. A total of 315 frames of 1° rotation each was collected on a single crystal. Overall radiation damage was evidenced by a steady decrease in average I/σ as a function of exposure time. The program HySS (Grosse-Kunstleve and Adams, 2003) was used to find an initial set of 20 Se sites based on anomalous differences truncated to 4.0 Å resolution. Refinement of the Se atoms and phasing were carried out with the program SHARP (Bricogne et al., 2003). Initial refinement of the Se sites was carried out against a completely merged dataset. Additional sites were included in the refinement after inspection of residual maps. The final substructure model comprises 23 Se atoms. The data were then split up into three sequential parts, corresponding, respectively, to merged data from data frames 1–90, 91–180, and 181–315. Separate occupancy factors of the Se atoms were refined for each of the three datasets. The positional and thermal parameters of each individual Se atom were constrained to remain identical across all three datasets. The refined values for most of the Se sites displayed a clear trend of decreasing occupancies across the three sequential datasets—a feature that we ascribed to site-specific radiation damage. The final phases were obtained by refining dose-dependent occupancies for the Se atoms on the scaled but unmerged data (Schiltz et al., 2004). These phases led to a significantly improved map, which was subjected to density modification with the program SOLOMON, resulting in a map that allowed manual building of the model.

Site-Directed Mutagenesis

Point mutants were introduced by using a PCR-based method in a pET15b-vector (His-tagged Ypa1), a pGEX-vector (GST-tagged Ypa1), and a pYes2-vector (Yeast transformation). A forward and reverse mutant primer was used (see Table S1).

PTPA/Ypa Assays as Activator and PPIase

$PP2A_i$ was purified from porcine brain as inactive complex of $PP2A_D$ with PME-1 (Longin et al., 2004). To a 20 μl mixture containing 1.2 to 1.5 U/ml potential PP2A activity and 1 mM ATP, 5 mM $MgCl_2$ in 20 mM TrisCl, 0.5 mM DTT (pH 7.5) was added 10 μl purified PTPA/Ypa1 (or mutants) in a serial (5–7×) dilution 1:3. After 10 min preincubation at 30°C, 10 μl ^{32}P labeled phosphorylase *a* with 33 μg/ml protamin and 16 mM ammonium sulfate was added, and after 10 min at 30°C, TCA-soluble ^{32}P was measured (see Van Hoof et al. [2005] for further details). Two controls were always included in duplicate: the maximal PP2A activity measured with a saturating amount of PTPA and MgATP (=100%) and a control without PTPA/Ypa (subtracted as blanco). One unit PTPA reactivates 30% $PP2A_i$ in this assay (see Figure S5 for some examples).

The PPIase activity of all mutants was routinely measured by using the suc-Ala-Ala-Pro-Lys-pNA substrate and the trypsin-assisted PPIase measurement according to Jordens et al. (2006). k_{obs} values were measured at 20°C [suc-AAPK-pNA] = 8.25 μM; 1 mM ATP, 5 mM $MgCl_2$; [Ypa1] = 0.5 μM; [trypsin] = 4.4 μM. All values are presented after subtraction of the blanco value, measured with addition of [BSA] = 0.4 μM (k_{obs} about 0,003 s^{-1}). In some cases, independent evidence of PPIase activity was sought by the band-shape analysis technique of the spectra in dynamic proton NMR spectrometry as described by Hübner et al. (1991) and performed as in Jordens et al. (2006) with 1 mM peptide (LQEVPHEGPMCDL), 5 μM Ypa1 (or mutant), and 2 mM ATP/10 mM $MgCl_2$ in otherwise the same conditions. For Ypa1, the band broadening is systematically lower than for the rabbit PTPA (see Figure 4 in Jordens et al. [2006]) for unknown reasons. Nevertheless, the changes can still be observed for the wild-type and P268A mutant in comparison with the control (no Ypa1), whereas this is not the case for the W202G and D205G mutants (Figure 5). Because this method give only qualitative results, these are shown in Figure 5 and appreciated in Table 2 with a Yes or No.

Yeast Transformation and Rapamycin Sensitivity

Figure S6 showing the growth on rapamycin of different mutated yeast strains and the concerning methods can be found in the Supplemental Data and is appreciated by + and − in Table 2.

Supplemental Data

Supplemental Data include Supplemental Experimental Procedures, Supplemental References, six figures, and one table and can be found with this article online at http://www.molecule.org/cgi/content/full/23/3/413/DC1/.

Acknowledgments

HvT thanks the Association pour la Recherché sur le Cancer for a research grant (number 3873). D.B.'s laboratory was funded by Cancer Research-United Kingdom and the Institute of Cancer Research. We are grateful to Drs. David Komander and Mark Roe for help with data collection and the staff at European Synchrotron Radiation Facility. J.G.'s laboratory was supported by the Fonds voor Wetenschappelijk onderzoek Vlaanderen, the Geconcerteerde Onderzoeksacties van de Vlaamse gemeenschap, the Interuniversity Attraction Poles programme, Belgian Science Policy, and by BioMaCS. We are grateful to M.R. Verbiest and M. Veeckmans for expert technical assistance and V. Feytons for peptide synthesis. We wish to thank T. Rose (Pasteur Institute, Paris) for the ultracentrifugation experiments and E. Lescrinier (BioMaCS, Leuven)for the ^{1}H-NMR-based PPIase measurements. M.S. acknowledges financial support from the Swiss National Science Foundation through grant number 200021-107637.

Received: March 6, 2006
Revised: June 12, 2006
Accepted: July 13, 2006
Published: August 3, 2006

References

Andreotti, A.H. (2003). Native state proline isomerization: an intrinsic molecular switch. Biochemistry *42*, 9515–9524.

Bricogne, G., Vonrhein, C., Flensburg, C., Schiltz, M., and Paciorek, W. (2003). Generation, representation and flow of phase information in structure determination: recent developments in and around SHARP 2.0. Acta Crystallogr. D Biol. Crystallogr. *59*, 2023–2030.

Brown, N.R., Noble, M.E., Endicott, J.A., and Johnson, L.N. (1999). The structural basis for specificity of substrate and recruitment peptides for cyclin-dependent kinases. Nat. Cell Biol. *1*, 438–443.

Cayla, X., Goris, J., Hermann, J., Hendrix, P., Ozon, R., and Merlevede, W. (1990). Isolation and characterization of a tyrosyl phosphatase activator from rabbit skeletal muscle and Xenopus laevis oocytes. Biochemistry *29*, 658–667.

Chen, J., Martin, B.L., and Brautigan, D.L. (1992). Regulation of protein serine-threonine phosphatase type-2A by tyrosine phosphorylation. Science *257*, 1261–1264.

De Baere, I., Derua, R., Janssens, V., Van Hoof, C., Waelkens, E., Merlevede, W., and Goris, J. (1999). Purification of porcine brain protein phosphatase 2A leucine carboxyl methyltransferase and cloning of the human homologue. Biochemistry *38*, 16539–16547.

Di Como, C.J., and Arndt, K.T. (1996). Nutrients, via the Tor proteins, stimulate the association of Tap42 with type 2A phosphatases. Genes Dev. *10*, 1904–1916.

Douville, J., David, J., Fortier, P.K., and Ramotar, D. (2004). The yeast phosphotyrosyl phosphatase activator protein, yPtpa1/Rrd1, interacts with Sit4 phosphatase to mediate resistance to 4-nitroquinoline-1-oxide and UVA. Curr. Genet. *46*, 72–81.

Fanghanel, J., and Fischer, G. (2004). Insights into the catalytic mechanism of peptidyl prolyl cis/trans isomerases. Front. Biosci. *9*, 3453–3478.

Favre, B., Zolnierowicz, S., Turowski, P., and Hemmings, B.A. (1994). The catalytic subunit of protein phosphatase 2A is carboxyl-methylated in vivo. J. Biol. Chem. *269*, 16311–16317.

Fellner, T., Lackner, D.H., Hombauer, H., Piribauer, P., Mudrak, I., Zaragoza, K., Juno, C., and Ogris, E. (2003). A novel and essential mechanism determining specificity and activity of protein phosphatase 2A (PP2A) in vivo. Genes Dev. *17*, 2138–2150.

Gouet, P., Courcelle, E., Stuart, D.I., and Metoz, F. (1999). ESPript: analysis of multiple sequence alignments in PostScript. Bioinformatics *15*, 305–308.

Grosse-Kunstleve, R.W., and Adams, P.D. (2003). Substructure search procedures for macromolecular structures. Acta Crystallogr. D Biol. Crystallogr. *59*, 1966–1973.

Groves, M.R., Hanlon, N., Turowski, P., Hemmings, B.A., and Barford, D. (1999). The structure of the protein phosphatase 2A PR65/A subunit reveals the conformation of its 15 tandemly repeated HEAT motifs. Cell *96*, 99–110.

Guo, H., and Damuni, Z. (1993). Autophosphorylation-activated protein kinase phosphorylates and inactivates protein phosphatase 2A. Proc. Natl. Acad. Sci. USA *90*, 2500–2504.

Harrison, R.K., and Stein, R.L. (1990). Mechanistic studies of peptidyl prolyl cis-trans isomerase: evidence for catalysis by distortion. Biochemistry *29*, 1684–1689.

Jacinto, E., and Hall, M.N. (2003). Tor signalling in bugs, brain and brawn. Nat. Rev. Mol. Cell Biol. *4*, 117–126.

Hübner, D., Drakenberg, T., Forsen, S., and Fischer, G. (1991). Peptidyl-prolyl cis-trans isomerase activity as studied by dynamic proton NMR spectroscopy. FEBS Lett. *284*, 79–81.

Janssens, V., and Goris, J. (2001). Protein phosphatase 2A: a highly regulated family of serine/threonine phosphatases implicated in cell growth and signalling. Biochem. J. *353*, 417–439.

Janssens, V., Van Hoof, C., De Baere, I., Merlevede, W., and Goris, J. (1999). Functional analysis of the promoter region of the human phosphotyrosine phosphatase activator gene: Yin Yang 1 is essential for core promoter activity. Biochem. J. *344*, 755–763.

Janssens, V., Van Hoof, C., De Baere, I., Merlevede, W., and Goris, J. (2000a). The phosphotyrosyl phosphatase activator gene is a novel p53 target gene. J. Biol. Chem. *275*, 20488–20495.

Janssens, V., Van Hoof, C., Martens, E., De Baere, I., Merlevede, W., and Goris, J. (2000b). Identification and characterization of alternative splice products encoded by the human phosphotyrosyl phosphatase activator gene. Eur. J. Biochem. *267*, 4406–4413.

Janssens, V., Goris, J., and Van Hoof, C. (2005). PP2A: the expected tumor suppressor. Curr. Opin. Genet. Dev. *15*, 34–41.

Jin, L., and Harrison, S.C. (2002). Crystal structure of human calcineurin complexed with cyclosporin A and human cyclophilin. Proc. Natl. Acad. Sci. USA *99*, 13522–13526.

Jordens, J., Janssens, V., Longin, S., Stevens, I., Martens, E., Bultynck, G., Engelborghs, Y., Lescrinier, E., Waelkens, E., Goris, J., and Van Hoof, C. (2006). The PP2A phosphatase activator (PTPA) is a novel peptidyl-prolyl cis/trans isomerase. J. Biol. Chem. *281*, 6349–6357.

Kaeberlein, M., Andalis, A., Liszt, G., Fink, G., and Guarente, L. (2004). *Saccharomyces cerevisiae SSD1-V* confers longevity by a Sirp-independent mechanism. Genetics *166*, 1661–1672.

Kong, M., Fox, C.J., Mu, J., Solt, L., Xu, A., Cinalli, R.M., Birnbaum, M.J., Lindsten, T., and Thompson, C.B. (2004). The PP2A-associated protein alpha4 is an essential inhibitor of apoptosis. Science *306*, 695–698.

Kremmer, E., Ohst, K., Kiefer, J., Brewis, N., and Walter, G. (1997). Separation of PP2A core enzyme and holoenzyme with monoclonal antibodies against the regulatory A subunit: abundant expression of both forms in cells. Mol. Cell. Biol. *17*, 1692–1701.

Lee, J.O., Russo, A.A., and Pavletich, N.P. (1998). Structure of the retinoblastoma tumour-suppressor pocket domain bound to a peptide from HPV E7. Nature *3912*, 859–865.

Leulliot, N., Quevillon-Cheruel, S., Sorel, I., de La Sierra-Gallay, I.L., Collinet, B., Graille, M., Blondeau, K., Bettache, N., Poupon, A., Janin, J., and van Tilbeurgh, H. (2004). Structure of protein phosphatase methyltransferase 1 (PPM1), a leucine carboxyl methyltransferase involved in the regulation of protein phosphatase 2A activity. J. Biol. Chem. *279*, 8351–8358.

Li, X., and Virshup, D.M. (2002). Two conserved domains in regulatory B subunits mediate binding to the A subunit of protein phosphatase 2A. Eur. J. Biochem. *269*, 546–552.

Longin, S., Jordens, J., Martens, E., Stevens, I., Janssens, V., Rondelez, E., De Baere, I., Derua, R., Waelkens, E., Goris, J., and Van Hoof, C. (2004). An inactive protein phosphatase 2A population is associated with methylesterase and can be re-activated by the phosphotyrosyl phosphatase activator. Biochem. J. *380*, 111–119.

McCright, B., Rivers, A.M., Audlin, S., and Virshup, D.M. (1996). The B56 family of protein phosphatase 2A (PP2A) regulatory subunits encodes differentiation-induced phosphoproteins that target PP2A to both nucleus and cytoplasm. J. Biol. Chem. *271*, 22081–22089.

Mitchell, D.A., and Sprague, G.F., Jr. (2001). The phosphotyrosyl phosphatase activator, Ncs1p (Rrd1p), functions with Cla4p to regulate the G(2)/M transition in Saccharomyces cerevisiae. Mol. Cell. Biol. *21*, 488–500.

Murata, K., Wu, J., and Brautigan, D.L. (1997). B cell receptor-associated protein alpha4 displays rapamycin-sensitive binding directly to the catalytic subunit of protein phosphatase 2A. Proc. Natl. Acad. Sci. USA *94*, 10624–10629.

Ogris, E., Du, X., Nelson, K.C., Mak, E.K., Yu, X.X., Lane, W.S., and Pallas, D.C. (1999). A protein phosphatase methylesterase (PME-1) is one of several novel proteins stably associating with two inactive mutants of protein phosphatase 2A. J. Biol. Chem. *274*, 14382–14391.

Rempola, B., Kaniak, A., Migdalski, A., Rytka, J., Slonimski, P.P., and di Rago, J.P. (2000). Functional analysis of RRD1 (YIL153w) and RRD2 (YPL152w), which encode two putative activators of the phosphotyrosyl phosphatase activity of PP2A in *Saccharomyces cerevisiae*. Mol. Gen. Genet. *262*, 1081–1092.

Schiltz, M., Dumas, P., Ennifar, E., Flensburg, C., Paciorek, W., Vonrhein, C., and Bricogne, G. (2004). Phasing in the presence of severe site-specific radiation damage through dose-dependent modelling of heavy atoms. Acta Crystallogr. D Biol. Crystallogr. *60*, 1024–1031.

Thompson, J.D., Higgins, D.G., and Gibson, T.J. (1994). CLUSTAL W: improving the sensitivity of progressive multiple sequence alignment through sequence weighting, position-specific gap penalties and weight matrix choice. Nucleic Acids Res. *22*, 4673–4680.

Usui, H., Inoue, R., Tanabe, O., Nishito, Y., Shimizu, M., Hayashi, H., Kagamiyama, H., and Takeda, M. (1998). Activation of protein phosphatase 2A by cAMP-dependent protein kinase-catalyzed phosphorylation of the 74-kDa B'' (delta) regulatory subunit in vitro and identification of the phosphorylation sites. FEBS Lett. *430*, 312–316.

Van Hoof, C., Aly, M.S., Garcia, A., Cayla, X., Cassiman, J.J., Merlevede, W., and Goris, J. (1995). Structure and chromosomal localization of the human gene of the phosphotyrosyl phosphatase activator (PTPA) of protein phosphatase 2A. Genomics *28*, 261–272.

Van Hoof, C., Janssens, V., Dinishiotu, A., Merlevede, W., and Goris, J. (1998). Functional analysis of conserved domains in the phosphotyrosyl phosphatase activator. Molecular cloning of the homologues from Drosophila melanogaster and Saccharomyces cerevisiae. Biochemistry *37*, 12899–12908.

Van Hoof, C., Janssens, V., De Baere, I., de Winde, J.H., Winderickx, J., Dumortier, F., Thevelein, J.M., Merlevede, W., and Goris, J. (2000). The Saccharomyces cerevisiae homologue YPA1 of the mammalian phosphotyrosyl phosphatase activator of protein phosphatase 2A controls progression through the G1 phase of the yeast cell cycle. J. Mol. Biol. *302*, 103–120.

Van Hoof, C., Janssens, V., De Baere, I., Stark, M.J., de Winde, J.H., Winderickx, J., Thevelein, J.M., Merlevede, W., and Goris, J. (2001). The Saccharomyces cerevisiae phosphotyrosyl phosphatase activator proteins are required for a subset of the functions disrupted by protein phosphatase 2A mutations. Exp. Cell Res. *264*, 372–387.

Van Hoof, C., Martens, E., Longin, S., Jordens, J., Stevens, I., Janssens, V., and Goris, J. (2005). Specific interactions of PP2A and PP2A-like phosphatases with the yeast PTPA homologues, Ypa1 and Ypa2. Biochem. J. *386*, 93–102.

Vogel, M., Bukau, B., and Mayer, M.P. (2006). Allosteric regulation of hsp70 chaperones by a proline switch. Mol. Cell *21*, 359–367.

Zabrocki, P., Van Hoof, C., Goris, J., Thevelein, J.M., Winderickx, J., and Wera, S. (2002). Protein phosphatase 2A on track for nutrient-induced signalling in yeast. Mol. Microbiol. *43*, 835–842.

Zheng, Y., and Jiang, Y. (2005). The yeast phosphotyrosyl phosphatase activator is part of the Tap42-phosphatase complexes. Mol. Biol. Cell *16*, 2119–2127.

Accession Numbers

The PDB entry names are for the human PTPA, 2ixm; for Ypa2, 2ixn; for Ypa1, 2ixo; and for the Ypa1 complex, 2ixp.